Discordance between eNOS phosphorylation and activation revealed by multispectral imaging and chemogenetic methods

Emrah Eroglu[a,1,2], Seyed Soheil Saeedi Saravi[a,1], Andrea Sorrentino[a], Benjamin Steinhorn[a], and Thomas Michel[a,3]

[a]Division of Cardiovascular Medicine, Department of Medicine, Brigham and Women's Hospital, Harvard Medical School, Boston, MA 02115

Edited by Michael A. Marletta, University of California, Berkeley, CA, and approved August 28, 2019 (received for review June 26, 2019)

Nitric oxide (NO) synthesized by the endothelial isoform of nitric oxide synthase (eNOS) is a critical determinant of vascular homeostasis. However, the real-time detection of intracellular NO—a free radical gas—has been difficult, and surrogate markers for eNOS activation are widely utilized. eNOS phosphorylation can be easily measured in cells by probing immunoblots with phosphospecific antibodies. Here, we pursued multispectral imaging approaches using biosensors to visualize intracellular NO and Ca^{2+} and exploited chemogenetic approaches to define the relationships between NO synthesis and eNOS phosphorylation in cultured endothelial cells. We found that the G protein-coupled receptor agonists adenosine triphosphate (ATP) and histamine promoted rapid increases in eNOS phosphorylation, as did the receptor tyrosine kinase agonists insulin and Vascular Endothelial Growth Factor (VEGF). Histamine and ATP also promoted robust NO formation and increased intracellular Ca^{2+}. By contrast, neither insulin nor VEGF caused any increase whatsoever in intracellular NO or Ca^{2+}—despite eliciting strong eNOS phosphorylation responses. Our findings demonstrate an unexpected and striking discordance between receptor-modulated eNOS phosphorylation and NO formation in endothelial cells. Previous reports in which phosphorylation of eNOS has been studied as a surrogate for enzyme activation may need to be reassessed.

signal transduction | nitric oxide synthase | endothelial cells | phosphorylation

Nitric oxide (NO) is a short-lived free radical gas that subserves a broad range of cellular functions in cardiovascular cells and tissues (1). The rapid reaction of NO with other radical species and with transition metals facilitates its detection in cell-free systems using sensitive spectroscopic and chemiluminescent methods (2). Yet the reactivity of NO also serves to undermine its accurate detection in living cells, where NO readily forms adducts and metabolites within the complex intracellular milieu of reactive biomolecules. Over the years, many methods and assays have been developed to study the biological roles of NO in cells and tissues (3). However, the direct detection of the low physiological concentrations of NO that are present in cardiovascular cells represents a significant bioanalytical challenge (4).

Instead of measuring the unstable NO radical itself, some cell-based assays have relied on the detection of stable NO metabolites such as nitrite (NO_2^-) (5) or nitrosothiol (RSNO) (6) compounds. NO-sensitive electrodes have been developed (7), but their technical idiosyncrasies have undermined broader use. Another approach has been to quantitate nitric oxide synthase catalysis using the [^{3}H]-radiolabeled NOS substrate L-arginine and measuring its conversion to the product [^{3}H]-L-citrulline (8). Still other approaches have involved chemical and biological sensors, which vary in their sensitivity and specificity for detection of NO (9). However, for many years, the most commonly used approach to analyze the endothelial isoform of nitric oxide synthase (eNOS) activation in endothelial cells has been to probe immunoblots using commercially available phosphospecific antibodies that detect eNOS phosphorylation (10).

eNOS is a calcium/calmodulin-dependent enzyme (11) that undergoes phosphorylation at multiple sites, including serine, threonine, and tyrosine residues (12). Phosphorylation at some sites is associated with enzyme activation, and phosphorylation at other sites has been correlated with inhibition of eNOS activity (13). The most extensively studied eNOS phosphorylation site is serine 1177 (S1177) (14). Phosphorylation of eNOS at S1177 in endothelial cells has been observed in response to activation of dozens of different cell surface receptors (14). Evidence for eNOS activation following S1177 phosphorylation is abundant, yet largely circumstantial (15, 16). Studies using purified eNOS "phosphomimetic" mutants—in which aspartic acid was substituted for serine (S1177D)—were claimed to be "constitutively active" based on in vitro analyses of selected kinetic features of the purified protein (10). Transgenic mice expressing the eNOS S1177D mutant appear to have enhanced endothelium-dependent vasodilation, while "phospho-null" S1177A mutant mice are hypertensive (17); these findings are consistent with more NO production by the S1177D eNOS mutant and less by the S1177A mutant (16). The eNOS S1177 site can be phosphorylated by a very broad array of different protein kinases (13, 16, 18–21) that are activated by diverse cell receptors (13), including G protein-coupled receptors for histamine and adenosine triphosphate (ATP), as well as receptor tyrosine kinases that bind growth factors, including Vascular Endothelial Growth Factor (VEGF) and insulin. At least 10 different biotech companies market phosphospecific antibodies that can be used to probe immunoblots for phospho-eNOS^{1177} and more than 2,000 papers in PubMed (including papers from our

Significance

Nitric oxide (NO) is synthesized by the endothelial isoform of nitric oxide synthase (eNOS) in vascular endothelial cells. The high reactivity of NO undermines its accurate detection in living cells. The direct detection of the low physiological concentrations of NO that are present in endothelial cells represents a significant analytical challenge. In these studies, we have used powerful biosensors to measure NO and other key signaling molecules in living endothelial cells in real time using fluorescence microscopy. These approaches have provided insights into the mechanisms whereby NO synthesis is regulated and call into question many prior conclusions about the intracellular pathways that regulate eNOS.

Author contributions: E.E., S.S.S.S., A.S., B.S., and T.M. designed research; E.E., S.S.S.S., and A.S. performed research; E.E. and B.S. contributed new reagents/analytic tools; E.E., S.S.S.S., A.S., and T.M. analyzed data; and E.E., S.S.S.S., and T.M. wrote the paper.

The authors declare no conflict of interest.

This article is a PNAS Direct Submission.

[1]E.E. and S.S.S.S. contributed equally to this work.

[2]Present address: Faculty of Engineering and Natural Sciences, Molecular Biology, Genetics and Bioengineering Program, Sabanci University, Orhanli-Tuzla, 34956 Istanbul, Turkey.

[3]To whom correspondence may be addressed. Email: thomas_michel@hms.harvard.edu.

This article contains supporting information online at www.pnas.org/lookup/suppl/doi:10.1073/pnas.1910942116/-/DCSupplemental.

First published September 16, 2019.

laboratory; refs. 22–24) have reported studies analyzing eNOS phosphorylation at this site. At the risk of confounding association with causation, the hypothesis that eNOS S1177 phosphorylation represents a marker for enzyme activation seems plausible. However, our current findings provide evidence that this interpretation may be ill-founded in many contexts.

Here, we have exploited multispectral imaging approaches using sensitive and specific biosensors to quantitate intracellular NO in real time in living endothelial cells in order to define the relationship between NO synthesis and eNOS phosphorylation. These studies have revealed a striking discordance between receptor-dependent eNOS phosphorylation and NO synthesis in cultured endothelial cells.

Results

Multispectral Imaging of Ca^{2+} and NO in Single Endothelial Cells. The analysis of biosensors with distinct spectral properties permits multiparametric imaging at the level of individual cells. For the experiments shown here, we utilized spectral variants of the recently developed geNOp biosensor (25–29). This class of single fluorescent protein-based NO biosensors has been shown to be highly specific and sensitive for NO in a nanomolar range, but not to other reactive nitrogen and oxygen species such as peroxynitrite ($ONOO^-$), superoxide (O_2^-), carbon monoxide (CO), nitrite (NO_2^-), nitrate (NO_3^-), and hydrogen peroxide (H_2O_2) (26). We studied this NO biosensor along with the well-established Ca^{2+} indicator GECO (30) in order to simultaneous image Ca^{2+} and NO in single endothelial cells. Because the fluorescence emission profile of geNOp containing cyan fluorescent protein ("C-geNOp") can be easily distinguished from the emission pattern of the red fluorescent protein-based GECO ("R-GECO"), this combination was utilized for dual color imaging. We studied these biosensors in the human endothelial cell line EA.hy926 (31), which is derived from human umbilical vein endothelial cells. EA.hy926 cells have been extensively characterized and validated for the analysis of eNOS (32). EA.hy926 cells were cotransfected with plasmids encoding the NO biosensor C-geNOp and the Ca^{2+} indicator R-GECO. Fig. 1 shows spectra of cotransfected EA.hy926 cells imaged after addition of ATP, which activates the G protein-coupled P2Y2 receptor in these cells (33). ATP treatment resulted in a rapid increase in Ca^{2+} levels (detected by R-GECO) followed by a robust rise in NO levels (detected by C-geNOp). Removing ATP from the superfusion buffer led to a rapid return of the Ca^{2+} and NO signals to basal levels (Fig. 1). These results document a close temporal relationship between agonist-modulated increases in intracellular Ca^{2+} and the formation of NO in single endothelial cells.

Characterizing Agonist-Mediated eNOS Phosphorylation and NO Synthesis. We next explored eNOS phosphorylation following treatment of EA.hy926 cells with agonists that activate cell surface receptors that have been linked to eNOS responses in these cells (31). The cells were treated with 2 GPCR agonists—ATP and histamine—as well as with 2 receptor tyrosine kinase agonists, VEGF, and insulin. Following agonist treatments of EA.hy926 cells, cell lysates were probed with phosphospecific antibodies that recognize individual eNOS phosphorylation sites (Fig. 2). All 4 agonists promoted similar levels of phosphorylation of eNOS at S1177. An independent antibody (from Millipore) against S1177 gave quantitatively identical results as the Cell Signaling Technology antibody used in these studies (*SI Appendix*, Fig. S1). Neither S114 nor T495 showed significant changes in phosphorylation following agonist treatments in these cells. Our subsequent experiments, therefore, focused on the study of agonist-modulated phosphorylation of eNOS at S1177.

We explored the relationship between eNOS S1177 phosphorylation and eNOS activation using the C-geNOp and R-GECO biosensors to detect NO and Ca^{2+}, respectively. Fig. 3 shows the results of multispectral real-time imaging of EA.hy926 cells cotransfected with the NO-sensitive C-geNOp biosensor along with the Ca^{2+} indicator R-GECO. Both ATP and histamine stimulated significant increases in intracellular NO and Ca^{2+}. When the agonists were withdrawn from the cells, the NO and Ca^{2+} signals returned to baseline levels. In parallel experiments conducted with the same cells (Fig. 3), we found that both histamine and ATP stimulated robust eNOS phosphorylation at S1177. However, when we analyzed biosensor responses to VEGF and insulin, we were surprised to discover neither VEGF nor insulin promoted any increases whatsoever in NO or Ca^{2+}, despite promoting equally robust eNOS S1177 phosphorylation as ATP and histamine (Fig. 3). Thus, while all 4 agonists (ATP, histamine, insulin, and VEGF) promoted similar levels of eNOS S1177 phosphorylation, only ATP and histamine treatments increased NO and Ca^{2+} in these cells. Insulin and VEGF failed entirely to increase either NO or Ca^{2+}, while still promoting robust eNOS S1177 phosphorylation. These findings demonstrate a discordance between agonist-modulated eNOS phosphorylation and eNOS activation. To corroborate our findings using geNOp imaging to detect NO, we also measured agonist-modulated NO responses using the well-established Griess assay for nitrite/nitrate detection. As was found in the geNOp imaging, the Griess assay revealed that treatment of EA.hy926 cells with either ATP or histamine yielded significant nitrate increases, but there was no nitrate response to either VEGF or insulin (*SI Appendix*, Fig. S2). In additional control experiments, we found no significant changes in agonist-stimulated phosphorylation responses when cells were incubated in the same buffer as was used for imaging experiment (*SI Appendix*, Fig. S3).

Cytosolic Ca^{2+} Elevation Is Essential for eNOS Activation in EA.hy926 Cells. Pretreatment of cells with the NOS inhibitor N^{ω}-nitro-L-arginine (L-NNA) before the imaging experiments completely

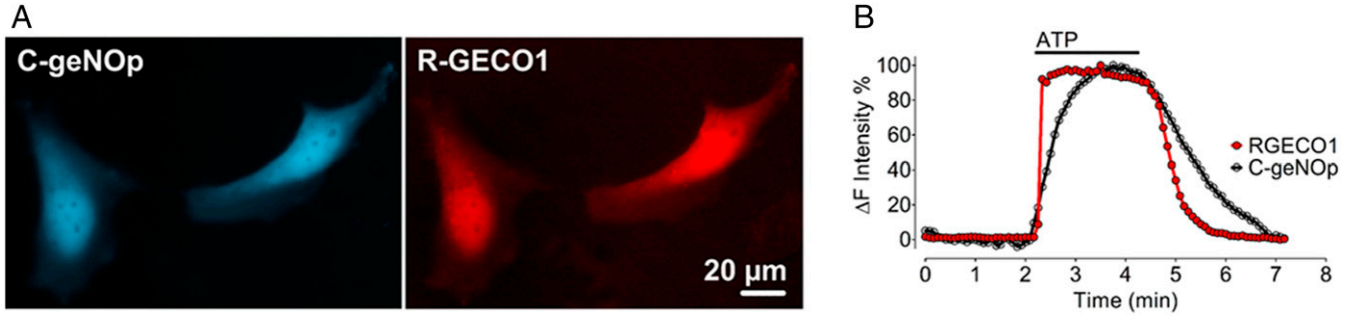

Fig. 1. Multispectral single-cell imaging of NO and Ca^{2+} signals. (*A*) Pseudocolored representative widefield images of EA.hy926 cells coexpressing the cyan fluorescent protein-based NO probe C-geNOp and the red fluorescent protein-based R-GECO. (*B*) Representative time course of intracellular Ca^{2+} (red curve) and NO (black curve) of a single EA.hy926 cell in response to 30 μM ATP.

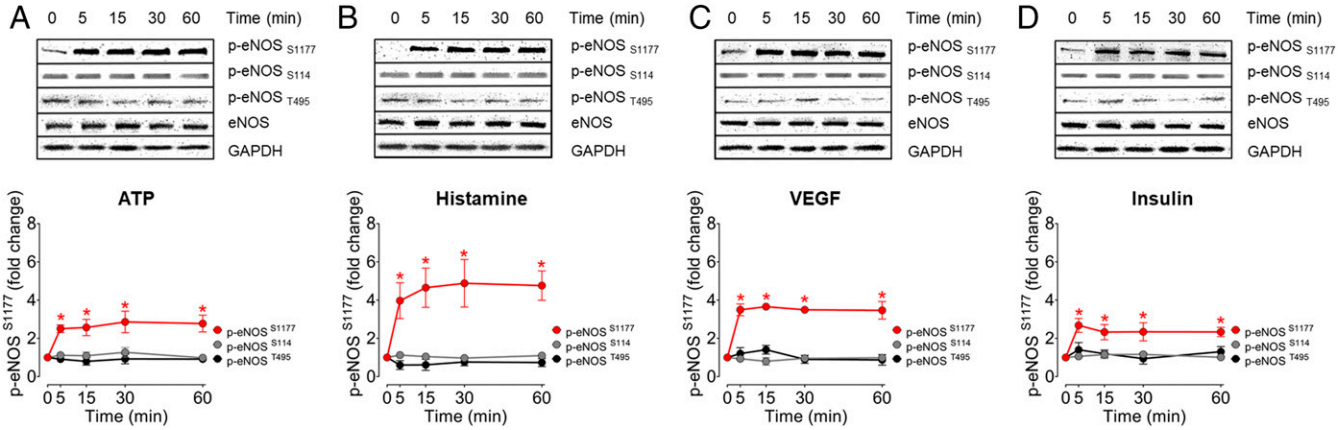

Fig. 2. Agonist-mediated eNOS phosphorylation patterns in EA.hy926 endothelial cells. (*A–D*) Representative immunoblots of time course experiments in EA.hy926 endothelial cells (*Upper*) treated with ATP, histamine, VEGF, or insulin. Cell lysates were probed with antibodies directed against eNOS phosphorylation sites at Ser1177, Ser114, and Thr495. Cell lysates were also probed for total eNOS as a loading control. (*Lower*) The pooled data from time course experiments represent quantitative analysis of the intensities corresponding to phospho-eNOS at Ser^{1177}, Ser^{114}, and Thr^{495} by chemiluminescence. All experiments were performed in triplicate. All values are presented as mean ± SD, $*P < 0.001$ versus control using ANOVA and Tukey's multiple comparison test.

abrogated the C-geNOp signal without affecting the Ca^{2+} response to both histamine and ATP. Pretreatment of cells with the Ca^{2+} chelator 1,2-bis(*o*-aminophenoxy)ethane-*N*,*N*,*N*′,*N*′-tetra-acetic acid (BAPTA) completely blocked ATP or histamine-stimulated Ca^{2+} responses and prevented NO generation (Fig. 4). The specificity of the Ca^{2+} response was confirmed using the dye Fura-2/AM (*SI Appendix*, Fig. S5). Taken together, these results help to further validate the specificity of the C-geNOp biosensor and also serve to demonstrate the necessity of receptor-modulated Ca^{2+} increases for the generation of NO.

Chemogenetic Generation of H_2O_2 Leads to eNOS S1177 Phosphorylation but Not to NO Formation. The stable reactive oxygen species (ROS) H_2O_2 has been extensively studied as an intracellular signaling molecule in endothelial cells (34). H_2O_2 modulates intracellular phosphorylation pathways and has a significant effect on eNOS (35–37). We next used chemogenetic approaches to study the effects of ROS H_2O_2 on NO and Ca^{2+} responses in these cells. We utilized a recently developed chemogenetic approach that exploits a yeast D-amino acid oxidase (37–39) (DAAO) to generate H_2O_2 in these cells (Fig. 5*A*). Since endothelial cells contain L-amino acids but not D-amino acids, the enzyme remains quiescent until D-amino acids are provided to the cells (38). We cloned a chimeric construct consisting of DAAO and the H_2O_2 biosensor HyPer so that we could both generate (DAAO) and detect (HyPer) H_2O_2 in these cells (38).

The plasmid-based biosensors that we used in imaging experiments (Figs. 1–4) worked well for imaging studies, but for biochemical analyses, we needed to utilize a high-efficiency gene expression system. Adenovirus serotype 5 (AV5) can infect cells from the cardiovascular system with high efficiency (27, 39–41). We cloned the DAAO-HyPer construct into AV5 to generate the recombinant virus AV5-DAAO-HyPer and validated this recombinant construct in EA.hy926 cells (*SI Appendix*, Fig. S6 and Movie S1). Two days following infection of EA.hy926 cells with the chimeric AV5-DAAO-HyPer virus, we added either D-alanine or L-alanine to the cells. As shown in Fig. 5*B*, addition of D-alanine led to a robust increase in phosphorylation of eNOS at S1177; L-alanine had no effect. Next, we cotransfected EA.hy926 cells with HyPer-DAAO and R-GECO (in separate plasmid constructs) for multispectral imaging of H_2O_2 and Ca^{2+}. Addition of D-alanine led to a robust increase in intracellular H_2O_2 detected by the HyPer biosensor (Fig. 5*C*). However, the R-GECO signals remained unaffected by D-alanine treatment. Subsequent stimulation of the cotransfected cells with histamine confirmed that the Ca^{2+}-sensitive indicator remained responsive under these conditions (Fig. 5*C*). We then cotransfected EA.hy926 cells with HyPer-DAAO and the orange fluorescent protein-based variant of geNOp (termed O-geNOp), which permits simultaneous detection of the green HyPer signal along with the orange O-geNOp signal (*SI Appendix*, Fig. S7). EA.hy926 cells cotransfected with DAAO-HyPer and O-geNOp were treated with D-alanine, which led to a rapid increase in H_2O_2, yet there was no NO response in these cells (Fig. 5*D*). However, when these same cells were subsequently treated with histamine, there was a robust NO signal detected by O-geNOp (Fig. 5*D*). Taken together, these observations establish that H_2O_2-stimulated eNOS phosphorylation at S1177 does not lead to eNOS activation in these cells.

Effects of the AMPK Inhibitor Compound C on eNOS Phosphorylation and NO Production. One of the key protein kinases modulating eNOS phosphorylation is the AMP-activated protein kinase (AMPK) (42). We used the AMPK inhibitor Compound C to explore the relationship between AMPK-modulated eNOS phosphorylation and NO generation in these cells. As shown in Fig. 6, the increase in eNOS phosphorylation elicited by both ATP and histamine was markedly attenuated by the treatment of cells with Compound C. However, in cells transfected with O-geNOp, we found that pretreatment of EA.hy926 cells with Compound C had no effect on ATP-promoted or histamine-promoted NO generation. Because the spectral properties of Compound C interfere with the C-geNOp signal, we instead imaged NO responses with O-geNOp. However, the spectral properties of O-geNOp interfere with detection of the Ca^{2+} response using R-GECO, and so we used the well-characterized Ca^{2+} dye Fura2-AM for calcium measurements following Compound C treatments. As shown in Fig. 6*B*, Compound C has no effect on the ATP-stimulated or histamine-stimulated Ca^{2+} response (Fig. 6*B*). These results demonstrate that blockade of eNOS S1177 phosphorylation by the AMPK inhibitor Compound C does not affect either receptor-dependent eNOS activation or Ca^{2+} mobilization in these cells.

Studies in Bovine Aortic Endothelial Cells. We next sought to confirm our key findings in primary endothelial cells. We repeated several experiments in primary bovine aortic endothelial cells (BAEC), which have been utilized by many laboratories over many years (43) as a cultured endothelial cell model system for studying eNOS regulation. Bovine eNOS undergoes phosphorylation at S1179, which corresponds to S1177 in the human eNOS sequence. We performed multispectral imaging experiments in BAEC by

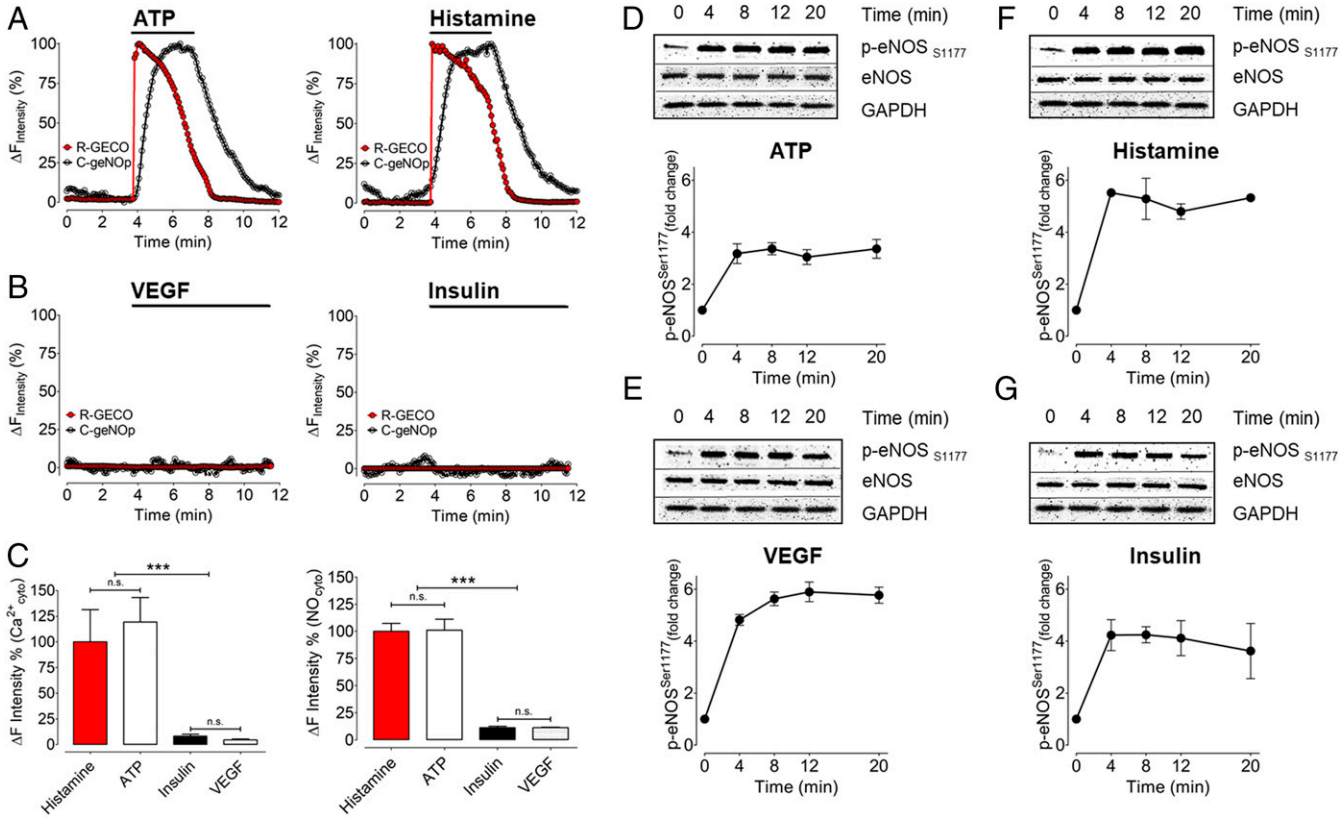

Fig. 3. Correlating multispectral imaging for NO and Ca^{2+} with eNOS phosphorylation. (*A*) Representative time course of intracellular Ca^{2+} (red curve) and NO (black curve) of a single EA.hy.926 cell in response to 30 μM ATP (*Left*) and 10 μM histamine (*Right*). (*B*) Curves show VEGF (10 ng/mL, *Left*) and insulin (100 nM, *Right*) induced Ca^{2+} (red curve) and NO (black curve) signals. (*C*) Bars in *Left* represent relative quantification of R-GECO signals in response to histamine (red bar, $n = 3/7$), ATP (white bar, $n = 3/8$), insulin (black bar, $n = 3/17$), and VEGF (white dotted bar, $n = 3/14$). Bars in *Right* represent the maximal amplitude of C-geNOp signals in response to histamine (red bar, $n = 3/13$), ATP (white bar, $n = 3/11$), insulin (black bar, $n = 3/9$), and VEGF (white dotted bar, $n = 3/17$). Absolute quantification for geNOp responses between histamine and ATP yielded 8.87 ± 2.32% and 8.96 ± 2.98% for histamine and ATP, respectively. $^*P < 0.05$ compared with other groups using ANOVA and Tukey's multiple comparison test. (*D–G*) Representative immunoblots from time course experiments analyzed in cells treated with ATP, histamine, VEGF, and insulin for times as indicated. Immunoblots of cell lysates were probed with antibodies directed against phospho-eNOS Ser^{1177}. Equal loading was confirmed by immunoblotting with an antibody against total eNOS. The pooled data from 3 independent experiments represent the intensities corresponding to phospho-eNOS at Ser^{1177} by chemiluminescence. Values are presented as mean ± SD, $^{***}P < 0.001$ versus control using ANOVA and Tukey's multiple comparison test.

coexpressing C-geNOp and R-GECO and studied the NO and Ca^{2+} responses to ATP, histamine, VEGF, and insulin (*SI Appendix*, Fig. S4*A*). Human and bovine endothelial cells are known to express different cell surface receptors in culture, and we found that histamine did not yield any signaling responses in BAEC: ATP alone evoked robust NO and Ca^{2+} signals. Immunoblots probed with antibodies against eNOS 1177 (S1179 in bovine eNOS) showed that VEGF, insulin, and ATP promoted robust eNOS phosphorylation at this site, while histamine elicited no response (*SI Appendix*, Fig. S4*B*). As in EA.hy926 cells, studies in BAEC again revealed a striking discordance between receptor-modulated eNOS activation and eNOS phosphorylation.

Discussion

These studies have pursued multispectral imaging approaches using genetically encoded biosensors that detect NO and Ca^{2+} with high specificity and spatiotemporal resolution in live endothelial cells (Fig. 1). We used these imaging approaches to probe the role of phosphorylation in eNOS activation, studying both the GPCR agonists histamine and ATP, as well as the RTK agonists insulin and VEGF. All 4 agonists promoted the robust phosphorylation of eNOS at S1177 in the human endothelial cell line EA.hy926 (Fig. 2). We then analyzed the corresponding changes in agonist-promoted eNOS activation and Ca^{2+} mobilization using multispectral biosensor imaging in live endothelial cells (Fig. 3). We found that both histamine and ATP elicited a robust NO and Ca^{2+} response, whereas neither insulin nor VEGF stimulated any change whatsoever in intracellular NO or Ca^{2+}. Thus, there is a striking discordance between the phosphorylation of eNOS at its putative "stimulatory" Ser1177 phosphorylation site and eNOS activation. Another example of the divergence between eNOS phosphorylation and activation came from our experiments using the AMPK inhibitor Compound C. We found that Compound C entirely blocked agonist-promoted eNOS phosphorylation at S1177 but had no effect whatsoever on Ca^{2+} or eNOS responses in these cells (Fig. 6). These and the other experiments shown above argue against the notion that analyses of eNOS S1177 phosphorylation can be used as a surrogate for NO formation. The disconnect between eNOS phosphorylation and eNOS activation was also seen in BAEC (*SI Appendix*, Fig. S4), indicating that these findings are not limited to only one endothelial cell type, but may represent a factor to be considered in the study of eNOS responses in other endothelial cell systems.

We used the geNOp biosensor for NO and the GECO biosensor for Ca^{2+} to explore the pathways leading from agonist binding to eNOS activation. The agonist-modulated geNOp signal was completely blocked by the NOS inhibitor L-NNA, but L-NNA had no effect on the agonist-modulated Ca^{2+} response (Fig. 4). By

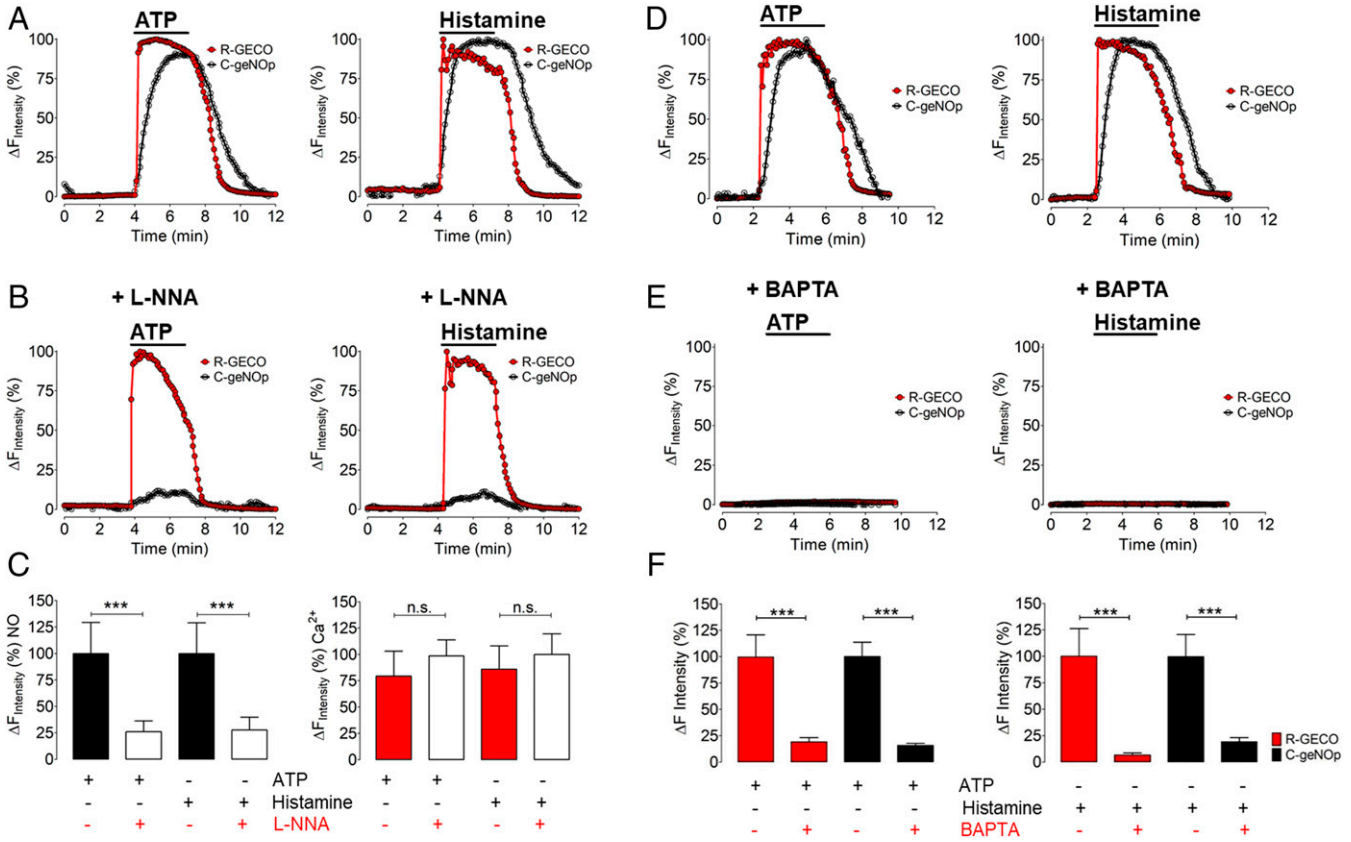

Fig. 4. Pharmacological inhibition of intracellular Ca^{2+} release and NO formation. (*A*) Representative time course of Eahy.926 cells coexpressing R-GECO1 and C-geNOp. Red curves represent cytosolic Ca^{2+}, and black curves represent NO signals in response to 30 μM ATP (*Left*) and 10 μM histamine (*Right*). (*B*) Graphs show the same experimental conditions, as shown in *A*. Cells were pretreated with 300 μM L-NNA for 30 min before the imaging experiment. (*C*) Bars of the *Left* represent maximal amplitude of C-geNOp signals in the absence of L-NNA and presence of ATP (black bar, $n = 3/11$), in the presence of ATP and L-NNA (white bar, $n = 3/12$), in response to histamine (white dotted bar, $n = 3/11$), and in the presence of histamine and L-NNA (gray dotted bar, $n = 3/14$). Bars in *Right* represent maximal amplitude of R-GECO1 signals in response to ATP (red bar, $n = 3/16$), in response to ATP and the presence of L-NNA (white bar, $n = 3/18$), in response to histamine (red dotted bar, $n = 3/16$), and in response to histamine in the presence of L-NNA (white dotted bar, $n = 3/18$). (*D*) Representative control experiments of intracellular Ca^{2+} (red curve) and NO (black curve) of a single EA.hy926 cell in response to 30 μM ATP (*Left*) and 10 μM histamine (*Right*). (*E*) Graphs show the same experimental conditions as in *D*. Cells were pretreated with 20 μM BAPTA for 45 min before the imaging experiment. (*F*) Bars in *Left* represent the maximal amplitude of R-GECO signals in the absence of BAPTA and presence of ATP (red bar, $n = 3/13$), in the presence of ATP and BAPTA (*Right* red bar, $n = 3/7$). Black bars in *Left* represent maximal C-geNOp signals in the presence of ATP (*Left* black bar, $n = 3/10$), and the presence of ATP and BAPTA (*Right* black bar, $n = 3/14$). Bars of *Right* represent the maximal amplitude of R-GECO signals in the absence of BAPTA and presence of histamine (red bar, $n = 3/13$), in the presence of histamine and BAPTA (*Right* red bar, $n = 3/11$). Black bars in *Right* represent maximal C-geNOp signals in the presence of histamine (*Left* black bar, $n = 3/13$), and the presence of histamine and BAPTA (*Right* black bar, $n = 3/7$). ***$P < 0.05$ compared with other groups using ANOVA and Tukey's multiple comparison test.

contrast, the intracellular calcium chelator BAPTA blocked both agonist-modulated eNOS activation and suppressed the Ca^{2+} signal (Fig. 4). These observations help to validate the specificity of these biosensors and are consistent with the known Ca^{2+} and arginine dependency of receptor-modulated eNOS activation.

Because of the important role of H_2O_2 in eNOS regulation (34), we used chemogenetic approaches to dynamically modulate intracellular H_2O_2 levels (Fig. 5). We found that chemogenetic generation of H_2O_2 using DAAO led to robust H_2O_2 generation along with a marked rise in eNOS phosphorylation at S1177. Once again, there was a striking discordance between eNOS phosphorylation and activation: Chemogenetic generation of H_2O_2 caused a significant increase in eNOS phosphorylation but failed entirely to increase intracellular Ca^{2+} or to activate eNOS. These observations stand in contrast to a previous study (44) in primary endothelial cells, in which addition of supraphysiological concentrations of extracellular H_2O_2 led both to eNOS phosphorylation as well as an increase in eNOS activity (assayed using the [^{3}H]-L-arginine/[^{3}H]-L-citrulline eNOS assay). This apparent discrepancy may simply reflect differences in cell type being studied (bovine vs. porcine endothelial cells) or differences in the NOS assays that were used. There may also be differences in the eNOS response elicited by the chemogenetic generation of intracellular H_2O_2 (as in the current studies) vs. the addition of H_2O_2 to the extracellular medium (as used in the prior report; ref. 44). In any event, our findings with H_2O_2 again raise an important caveat about drawing conclusions at the activation of eNOS from the experimental observation of eNOS phosphorylation.

What other roles could eNOS S1177 phosphorylation be playing in endothelial cells? One interesting clue comes from studies of purified eNOS: After in vitro eNOS phosphorylation at S1177, eNOS generated more superoxide than did the unphosphorylated enzyme, but the enzyme still remained dependent on Ca^{2+}/calmodulin. One caveat in interpreting these in vitro data are that the purified eNOS that was studied had been isolated from *Escherichia coli* and lacked the key posttranslational modifications that target mammalian eNOS to cell membranes (11). Indeed, eNOS undergoes an astonishing array of posttranslational modifications (11), interacts with multiple protein partners (11), and translocates from one region of the cell to another upon prolonged agonist activation (45). eNOS undergoes phosphorylation on S1177 when the enzyme is targeted to plasmalemmal caveolae, but not when

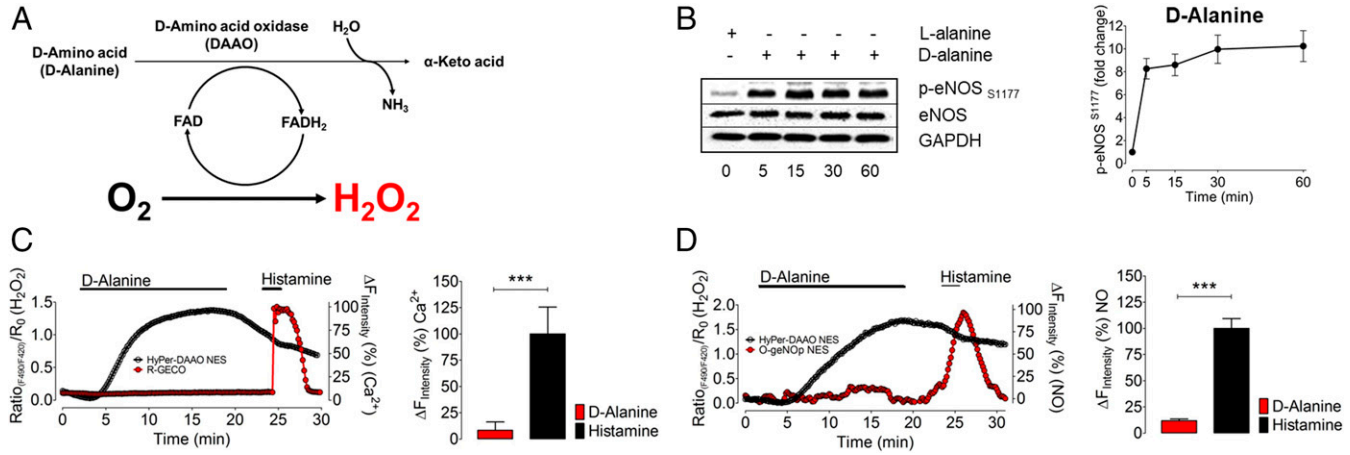

Fig. 5. Chemogenetic H_2O_2 production and multispectral imaging of H_2O_2, Ca^{2+}, and NO. (*A*) The schematic shows the DAAO catalytic pathway that oxidizes D-amino acids into keto acids and produces equimolar H_2O_2. (*B*) Representative immunoblots show time course experiments in EA.hy926 endothelial cells expressing DAAO-HyPer and incubated with 10 mM D-alanine (*Left*). *Right* presents pooled data from quantitative analysis of immunoblots probed with antibodies against phospho-eNOS^{1177}. Values are presented as mean ± SD, ***$P < 0.001$ versus control using ANOVA and Tukey's multiple comparison test. (*C, Left*) Representative time courses of a coimaging experiment of an Eahy.926 cell coexpressing R-GECO (red curve) and HyPer-DAAO (black curve). Cells were perfused with 10 mM D-alanine and 10 μM histamine for the indicated durations. (*Right*) Respective statistics for the maximum R-GECO response when treated with 10 mM D-alanine (red bar, $n = 3/8$) or 10 μM histamine (black bar, $n = 3/8$). (*D, Left*) The representative time course of a coimaging experiment of an EA.hy926 cell coexpressing O-geNOp (red curve) and HyPer-DAAO (black curve). Cells were perfused with 10 mM D-alanine and 10 μM histamine for the indicated times. (*Right*) Respective statistics for the maximum O-geNOp response when treated with 10 mM D-alanine (red bar, $n = 3/18$) or 10 μM histamine (black bar, $n = 3/18$). ***$P < 0.05$ versus control using the unpaired *t* test.

the enzyme is expressed in the cell cytosol (45). Perhaps eNOS S1177 phosphorylation modulates eNOS translocation or protein–protein associations or enzyme uncoupling. Our current studies have not distinguished among these possibilities. Other clues can be derived from studies of transgenic mice expressing "phosphomimetic" S1177D and "phosphonull" S1177A eNOS mutants, which were created on the background of eNOS knockout mice (46). There are important differences in vascular phenotype between the 2 phosphorylation mutants, suggesting that perhaps the biological consequences of eNOS phosphorylation are seen more clearly only over the longer term.

eNOS phosphorylation is neither necessary nor sufficient for eNOS activation. In vivo studies of eNOS phosphorylation mutants point to a complex vascular phenotype, and in vitro studies

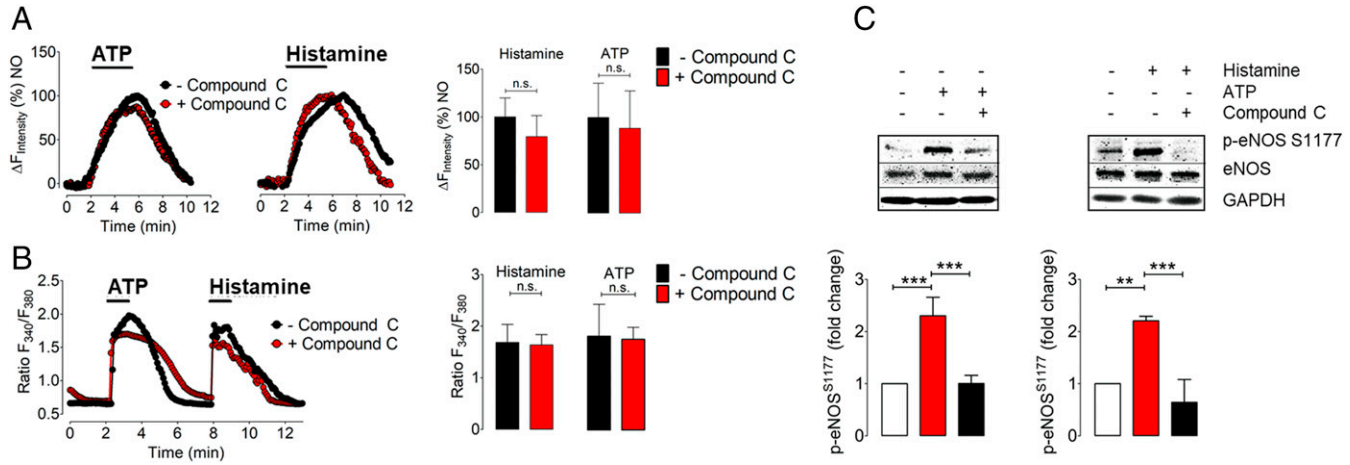

Fig. 6. Differential effects of Compound C on eNOS S1177 phosphorylation and NO formation. (*A, Left* and *Middle*) Representative time courses of NO signals in EA.hy.926 cells expressing the cytosolic orange variant of geNOps (O-geNOps) in response to 30 μM ATP (*Left*) and 10 μM histamine (*Middle*). Black curves represent control experiments while red curves represent NO responses of cells pretreated with Compound C (20 μM) before the experiment. (*Right*) Quantitative analysis of NO responses pretreated with Compound C (red bar, $n = 3/11$ for histamine, and $n = 3/10$ for ATP) and control conditions without any treatment (black bar, $n = 3/10$ for histamine, and $n = 3/9$ for ATP) (*B, Left*) Representative time course of cytosolic Ca^{2+} signals in response to ATP (30 μM) and, subsequently, histamine (10 μM) pretreated with Compound C for 20 min prior to the experiment (red curve) and without any pretreatment (black curve). Bars at *Right* represent the statistical analysis of the experiment shown in *Left*. Red bars represent cells pretreated with Compound C, $n = 3/35$ for ATP and histamine. Black bars represent control conditions, $n = 3/34$ for ATP, and histamine. n.s. indicates no statistical significance, unpaired *t* test. (*C*) Representative immunoblots are probing the consequences of AMPK inhibition on eNOS^{Ser1177} phosphorylation responses. EA.hy926 endothelial cells were incubated with the AMPK inhibitor, Compound C (20 μM) for 30 min before the stimulation with ATP (30 μM) or histamine (10 μM) for 8 min. Cell lysates were analyzed in immunoblots probed with the phosphospecific antibody directed against phosphorylation site of eNOS at Ser^{1177}. Equal loading was confirmed by immunoblotting with an antibody directed against total eNOS. Shown are pooled results analyzing the intensities corresponding to phospho-eNOS at Ser^{1177} by chemiluminescence from the independent experiments performed in triplicate. Values are presented as mean ± SD, **$P < 0.01$, ***$P < 0.001$ versus either control or Compound C-pretreated groups using ANOVA and Tukey's multiple comparison test.

identify multiple potential roles of S1177 in eNOS catalysis. Multispectral imaging of eNOS activation in live endothelial cells represents a powerful tool to dissect the signaling pathways that regulate this important vascular phosphoprotein. These studies have provided strong evidence that receptor-modulated eNOS phosphorylation responses can be dissociated from eNOS activation. Two decades on from the initial observations on the association between eNOS activation and eNOS phosphorylation, perhaps it is time to teach this old dogma some new tricks.

Conclusion

eNOS phosphorylation at S1177 has been studied and reported as a surrogate for eNOS activation in numerous publications since the discovery of eNOS phosphorylation at this site. We performed real-time multispectral imaging using sensitive biosensors in endothelial cells and documented a striking discordance between eNOS phosphorylation and eNOS activation. These findings affirm the importance of validating the enzymological consequences of protein phosphorylation in living cells and provide evidence that multispectral biosensor imaging methods can provide new insights into the control of intracellular signaling pathways.

Methods

Detailed methods are described in the *SI Appendix*.

Cell Culture, Plasmid Transfection, and Adenoviral Infection. EA.hy926 cells were obtained from American Type Culture Collection. Imaging experiments were performed 16 to 24 h after transfection. AV5-DAAO-HyPer expression in endothelial cells was achieved by adenoviral transduction at a multiplicity of infection of 1,000. Inquiry for biological reagents should be addressed to T.M. (thomas_michel@hms.harvard.edu) and E.E. (dr.emrah.eroglu@gmail.com).

Imaging Experiments. Cells transfected with geNOp constructs were incubated prior to the imaging experiment with an iron(II) fumarate solution before imaging. Ratiometric signals for HyPer were calculated by subtracting the background in each wavelength and calculating the ratio by dividing the intensity of the emission signals excited by 490 nm/420 nm. Real-time signals were acquired using Metafluor Software (Molecular Devices). For live-cell imaging, the number of experiments is indicated as "n = X/x", where X indicates the number of independent experiments and x indicates the total number of individual cells analyzed.

Immunoblot Analysis. After agonist treatments, the cells were washed with ice-cold phosphate-buffered saline and harvested with lysis buffer; immunoblot analyses of cell lysates were probed with antibodies and chemiluminescence signals analyzed using ImageJ software (NIH).

Statistical Analysis. Data are presented as mean values ± SEM. At least 3 different experiments have been performed for each condition.

ACKNOWLEDGMENTS. This work was supported by funds from National Institute on Aging of the National Institutes of Health Grant R21 AG06307 (to T.M.); National Diabetes, Digestive, and Kidney Diseases Institute of the National Institutes of Health Grant P30 DK057521 (to T.M.); National General Medical Sciences Institute of the National Institutes of Health Grant T32-GM007753 (to B.S.); a Brigham and Women's Hospital Health and Technology Innovation Award (to T.M.); American Diabetes Association Grant 9-17-CMF-012 (to A.S.); and Austrian Science Foundation Grant FWF J4113 (to E.E.).

1. D. Tousoulis, A.-M. Kampoli, C. Tentolouris, N. Papageorgiou, C. Stefanadis, The role of nitric oxide on endothelial function. *Curr. Vasc. Pharmacol.* **10**, 4–18 (2012).
2. N. S. Bryan, M. B. Grisham, Methods to detect nitric oxide and its metabolites in biological samples. *Free Radic. Biol. Med.* **43**, 645–657 (2007).
3. M. M. Tarpey, I. Fridovich, Methods of detection of vascular reactive species: Nitric oxide, superoxide, hydrogen peroxide, and peroxynitrite. *Circ. Res.* **89**, 224–236 (2001).
4. R. A. Hunter, W. L. Storm, P. N. Coneski, M. H. Schoenfisch, Inaccuracies of nitric oxide measurement methods in biological media. *Anal. Chem.* **85**, 1957–1963 (2013).
5. K. M. Miranda, M. G. Espey, D. A. A. Wink, A rapid, simple spectrophotometric method for simultaneous detection of nitrate and nitrite. *Nitric Oxide* **5**, 62–71 (2001).
6. J. S. Stamler *et al.*, Nitric oxide circulates in mammalian plasma primarily as an S-nitroso adduct of serum albumin. *Proc. Natl. Acad. Sci. U.S.A.* **89**, 7674–7677 (1992).
7. T. Malinski, Z. Taha, Nitric oxide release from a single cell measured in situ by a porphyrinic-based microsensor. *Nature* **358**, 676–678 (1992).
8. B. G. Hill, B. P. Dranka, S. M. Bailey, J. R. Lancaster, Jr, V. M. Darley-Usmar, What part of NO don't you understand? Some answers to the cardinal questions in nitric oxide biology. *J. Biol. Chem.* **285**, 19699–19704 (2010).
9. H. Kojima *et al.*, Detection and imaging of nitric oxide with novel fluorescent indicators: Diaminofluoresceins. *Anal. Chem.* **70**, 2446–2453 (1998).
10. D. Fulton *et al.*, Regulation of endothelium-derived nitric oxide production by the protein kinase Akt. *Nature* **399**, 597–601 (1999).
11. D. M. Dudzinski, T. Michel, Life history of eNOS: Partners and pathways. *Cardiovasc. Res.* **75**, 247–260 (2007).
12. V. Garcia, W. C. Sessa, Endothelial NOS: Perspective and recent developments. *Br. J. Pharmacol.* **176**, 189–196 (2019).
13. E. H. Heiss, V. M. Dirsch, Regulation of eNOS enzyme activity by posttranslational modification. *Curr. Pharm. Des.* **20**, 3503–3513 (2014).
14. C.-A. Chen, L. J. Druhan, S. Varadharaj, Y.-R. Chen, J. L. Zweier, Phosphorylation of endothelial nitric-oxide synthase regulates superoxide generation from the enzyme. *J. Biol. Chem.* **283**, 27038–27047 (2008).
15. P. F. Mount, B. E. Kemp, D. A. Power, Regulation of endothelial and myocardial NO synthesis by multi-site eNOS phosphorylation. *J. Mol. Cell. Cardiol.* **42**, 271–279 (2007).
16. S. Dimmeler *et al.*, Activation of nitric oxide synthase in endothelial cells by Akt-dependent phosphorylation. *Nature* **399**, 601–605 (1999).
17. D. N. Atochin, P. L. Huang, Endothelial nitric oxide synthase transgenic models of endothelial dysfunction. *Pflugers Arch.* **460**, 965–974 (2010).
18. V. A. Morrow *et al.*, Direct activation of AMP-activated protein kinase stimulates nitric-oxide synthesis in human aortic endothelial cells. *J. Biol. Chem.* **278**, 31629–31639 (2003).
19. B. J. Michell *et al.*, Coordinated control of endothelial nitric-oxide synthase phosphorylation by protein kinase C and the cAMP-dependent protein kinase. *J. Biol. Chem.* **276**, 17625–17628 (2001).
20. I. Fleming, B. Fisslthaler, S. Dimmeler, B. E. Kemp, R. Busse, Phosphorylation of Thr(^{495}) regulates Ca($^{2+}$)/calmodulin-dependent endothelial nitric oxide synthase activity. *Circ. Res.* **88**, E68–E75 (2001).
21. E. Butt *et al.*, Endothelial nitric-oxide synthase (type III) is activated and becomes calcium independent upon phosphorylation by cyclic nucleotide-dependent protein kinases. *J. Biol. Chem.* **275**, 5179–5187 (2000).
22. B. J. Kraus *et al.*, Novel role for retinol-binding protein 4 in the regulation of blood pressure. *FASEB J.* **29**, 3133–3140 (2015).
23. R. Bretón-Romero, H. Kalwa, S. Lamas, T. Michel, Role of PTEN in modulation of ADP-dependent signaling pathways in vascular endothelial cells. *Biochim. Biophys. Acta* **1833**, 2586–2595 (2013).
24. H. Kalwa *et al.*, Central role for hydrogen peroxide in P2Y1 ADP receptor-mediated cellular responses in vascular endothelium. *Proc. Natl. Acad. Sci. U.S.A.* **111**, 3383–3388 (2014).
25. E. Eroglu *et al.*, Development of novel FP-based probes for live-cell imaging of nitric oxide dynamics. *Nat. Commun.* **7**, 10623 (2016).
26. E. Eroglu *et al.*, Application of genetically encoded fluorescent nitric oxide (NO•) probes, the geNOps, for real-time imaging of NO• signals in single cells. *J. Vis. Exp.*, e55486 (2017).
27. E. Eroglu *et al.*, Real-time imaging of nitric oxide signals in individual cells using geNOps. *Methods Mol. Biol.* **1747**, 23–34 (2018).
28. E. Eroglu *et al.*, Genetic biosensors for imaging nitric oxide in single cells. *Free Radic. Biol. Med.* **128**, 50–58 (2018).
29. E. Eroglu *et al.*, Real-time visualization of distinct nitric oxide generation of nitric oxide synthase isoforms in single cells. *Nitric Oxide* **70**, 59–67 (2017).
30. Y. Zhao *et al.*, An expanded palette of genetically encoded Ca^{2+} indicators. *Science* **333**, 1888–1891 (2011).
31. K. Ahn, S. Pan, K. Beningo, D. Hupe, A permanent human cell line (EA.hy926) preserves the characteristics of endothelin converting enzyme from primary human umbilical vein endothelial cells. *Life Sci.* **56**, 2331–2341 (1995).
32. D. Bouïs, G. A. P. Hospers, C. Meijer, G. Molema, N. H. Mulder, Endothelium in vitro: A review of human vascular endothelial cell lines for blood vessel-related research. *Angiogenesis* **4**, 91–102 (2001).
33. A. Raqeeb, J. Sheng, N. Ao, A. P. Braun, Purinergic P2Y2 receptors mediate rapid $Ca^{(2+)}$ mobilization, membrane hyperpolarization and nitric oxide production in human vascular endothelial cells. *Cell Calcium* **49**, 240–248 (2011).
34. R. Bretón-Romero, S. Lamas, Hydrogen peroxide signaling in vascular endothelial cells. *Redox Biol.* **2**, 529–534 (2014).
35. H. Sies, Hydrogen peroxide as a central redox signaling molecule in physiological oxidative stress: Oxidative eustress. *Redox Biol.* **11**, 613–619 (2017).
36. E. A. Veal, A. M. Day, B. A. Morgan, Hydrogen peroxide sensing and signaling. *Mol. Cell* **26**, 1–14 (2007).
37. J. R. Stone, S. Yang, Hydrogen peroxide: A signaling messenger. *Antioxid. Redox Signal.* **8**, 243–270 (2006).
38. B. Steinhorn *et al.*, Chemogenetic generation of hydrogen peroxide in the heart induces severe cardiac dysfunction. *Nat. Commun.* **9**, 4044 (2018).
39. S. Charoensin *et al.*, Intact mitochondrial Ca^{2+} uniport is essential for agonist-induced activation of endothelial nitric oxide synthase (eNOS). *Free Radic. Biol. Med.* **102**, 248–259 (2017).
40. M. Opelt *et al.*, Formation of nitric oxide by aldehyde dehydrogenase-2 is necessary and sufficient for vascular bioactivation of nitroglycerin. *J. Biol. Chem.* **291**, 24076–24084 (2016).
41. M. Opelt *et al.*, Sustained formation of nitroglycerin-derived nitric oxide by aldehyde dehydrogenase-2 in vascular smooth muscle without added reductants: Implications for the development of nitrate tolerance. *Mol. Pharmacol.* **93**, 335–343 (2018).

42. Z. P. Chen *et al*., AMP-activated protein kinase phosphorylation of endothelial NO synthase. *FEBS Lett.* **443**, 285–289 (1999).
43. S. Shimizu, M. Ishii, T. Yamamoto, K. Momose, Mechanism of nitric oxide production induced by H_2O_2 in cultured endothelial cells. *Res. Commun. Mol. Pathol. Pharmacol.* **95**, 227–239 (1997).
44. S. R. Thomas, K. Chen, J. F. Keaney, Jr, Hydrogen peroxide activates endothelial nitric-oxide synthase through coordinated phosphorylation and dephosphorylation via a phosphoinositide 3-kinase-dependent signaling pathway. *J. Biol. Chem.* **277**, 6017–6024 (2002).
45. E. Gonzalez, R. Kou, A. J. Lin, D. E. Golan, T. Michel, Subcellular targeting and agonist-induced site-specific phosphorylation of endothelial nitric-oxide synthase. *J. Biol. Chem.* **277**, 39554–39560 (2002).
46. D. N. Atochin *et al*., The phosphorylation state of eNOS modulates vascular reactivity and outcome of cerebral ischemia in vivo. *J. Clin. Invest.* **117**, 1961–1967 (2007).